

Can one hear the shape of a Majorana Billiard?

Barış Pekerten,¹ A. Mert Bozkurt,¹ and İnanç Adagideli¹

¹*Faculty of Engineering and Natural Sciences, Sabancı University, Orhanlı-Tuzla, 34956 İstanbul, Turkey*

(Dated: May 12, 2022)

We study the fermion parity switches of the ground state of Majorana billiards, i.e. finitely sized, arbitrarily shaped superconducting islands that host Majorana fermions, where the superconductivity can either be inherent or induced via proximity effect. In particular, we study the density and statistics of these parity switches as a function of the applied magnetic field and chemical potential. We derive formulae that specify how the average density of parity switches depends on the geometrical size of the billiard as well as its boundary. Moreover, we show how the oscillations around this average value is determined by the classical periodic orbits of the billiard. Finally, we find that the statistics of the spacings of these parity switches are universal and are described by an appropriate random matrix ensemble, the choice of which depends on the antiunitary symmetries of the system in its normal state. We thus demonstrate that “one can hear (information about) the shape of a Majorana billiard” by investigating its “parity switch spectrum”.

PACS numbers: 73.22.-f, 74.78.Na, 74.20.Mn, 71.23.-k

I. INTRODUCTION

Eigenvalue spectra of finite quantum systems are related to their shape in the short wavelength limit^{1,2}. The celebrated Weyl expansion relates the smooth part of the density of states (DOS) to the volume, boundary area, curvature and Euler characteristics (number of handles) of the system^{2–4}. The remaining part, namely the DOS fluctuations, sensitively depends on the corresponding classical dynamics as well as the type of scattering featured in the system^{5–9}. Moreover, if all unitary symmetries are completely broken, the level-spacing distribution becomes universal and reflects the presence or absence of antiunitary symmetries^{8,10–14}.

The ground state of conventional, *s*-wave superconductors have an even number of fermions (i.e. even parity), reflecting their completely paired nature. However, under certain conditions, a state with an odd number of fermions (the odd parity state) can cross the even parity state to become the new ground state. This crossing is protected as the level repulsion due to perturbations that mix different fermion parity states are prohibited. While well known within the context of impurity states in superconductors^{15,16}, these crossings have attracted recent attention as they are zero dimensional counterparts to topological phase transitions^{17–28}. The two states at the transition point are the well known Majorana bound states which feature non-Abelian statistics^{29–34}, which have attracted intense recent attention as the candidate system for realization of topological quantum computers.

The presence of parity crossings has been regarded as the smoking gun signature of Majorana states in ballistic 1D wires^{35,36} and their universal statistics were first considered by Beenakker *et al.*²¹ Although there are strongly suggestive experimental spectral signatures^{37–40} of edge-bound zero bias states, conclusive experimental demonstration of the Majorana bound states has been elusive so far. The observed zero-bias conductance peaks could have non-topological origins such as Andreev

bound states^{26,27,41–57}, Kondo effect, weak antilocalization or disorder^{58–68}. In particular, recent experimental and theoretical work^{55,56,68} indicate multiple parity crossings in proximity coupled nanowires previously proposed to display topological superconductivity, as opposed to a window of parameters in which the topological properties are robust and an edge state is pinned to zero bias. Therefore, a better understanding of parity crossings in these proximity coupled systems is required.

In this work, we attempt at understanding fermion parity crossings in topological superconductors through the lens of spectral geometry, semiclassical physics and random matrix theory. We first focus on extracting geometrical information from the set of external parameters, which we call the “spectra” of parity crossings, at which the ground state fermion parity switches in a finite system. Such systems can be either finite sized superconductors, or normal-state regions coupled to superconductors (also known as Andreev billiards^{69–71}). We call these systems that feature parity switches “Majorana billiards” (MBs). In other words, we ask and answer the question whether one can “hear” the shape of a Majorana billiard from the “spectra” of parity crossings, alluding to Kac’s famous question, as phrased by L. Bers, “Can one hear the shape of a drum?”^{72,73}. To this end, we relate the parity crossing values of a MB to the real eigenvalues of another (fictional) non-Hermitian “Hamiltonian” under the assumption of the extent of at least one dimension of the system is much smaller than the superconducting coherence length ξ , and consider the Weyl expansion^{1–3} of the density of the spectra and its higher order terms.

In the same spirit, we next consider the oscillations around the asymptotic mean density of parity crossings. These semiclassical oscillations in the density of parity crossings, analogous to supershell effects in nuclear physics⁴, are experimentally accessible⁵⁵ and allow for a better understanding of the system. We stress that to the best of our knowledge there has been no theoretical investigation of these supershell effects so far. Finally,

we consider the statistics of parity crossing spacings for generic shapes and show they depend on whether the underlying normal system is regular, diffusive, chaotic or localized.

We note that the spectrum of parity crossings is experimentally accessible, as seen in recent experimental work⁵⁵. It is compelling to use our results to analyze experimental data relating to parity crossing spectra, especially from the point of shell and supershell effects and the bunching and antibunching of the parity crossing points. Our approach thus provides an extra point of view in understanding spectral measurements in proximity coupled TS systems.

Our manuscript is organized as follows: In Section II, we describe the *s*-wave and *p*-wave Majorana billiards which we discuss throughout the work. In Section III, we describe the mapping of MBs to normal systems and their analysis as an example of the Weyl problem (Figure 2). We next consider the supershell effects in the context of MB parity crossings (Fig. 3). Finally, we investigate the universal statistics of parity crossing distances (Fig. 4 and 5). We note that the numerical work presented in this manuscript show an excellent agreement with out analytical results without using any fitting parameters or any approximations beyond those of the traditional $k \cdot p$ Bogoliubov–de Gennes (BdG) Hamiltonian^{74–76} in a tight-binding setting.

II. DESCRIPTION OF THE SYSTEM

We consider finite 2D MB systems whose dynamics are described by the BdG Hamiltonian:

$$H_s = h(\mathbf{p}, \mathbf{r}) \tau_z + \alpha(p_x \sigma_y - p_y \sigma_x) \tau_z + B \sigma_x + \Delta \tau_x. \quad (1)$$

Here, σ_i [τ_i] are the Pauli matrices in spin [particle-hole] space with $i = x, y, z$, $h(\mathbf{p}, \mathbf{r}) = p^2/2m + V(\mathbf{r}) - \mu$ is the spinless part of the single-particle Hamiltonian with \mathbf{r} a point in the system, α is the spin-orbit interaction (SOI) constant, B is the Zeeman field and Δ is the *s*-wave pairing potential. $V(\mathbf{r})$ is the on-site, single-particle potential which includes disorder and confinement potentials. The systems can be clean or disordered, and their geometry could lead to chaotic or integrable dynamics in the classical limit (Fig. 1). We will also discuss the so-called depleted range of H_s , where the Zeeman field is large enough to deplete one of the spin-split bands^{75,76}. This range is described by the Hamiltonian

$$H_p = h(\mathbf{p}, \mathbf{r}) \tau_z + \Delta' \boldsymbol{\tau} \cdot \mathbf{p}, \quad (2)$$

where $\Delta' = \alpha \Delta / \epsilon$ is the effective SOI strength, with $\epsilon = \sqrt{B^2 - \Delta^2}$ for $B > \Delta$. Throughout this manuscript, we call systems featuring H_s (H_p) “*s*-wave” (“*p*-wave”). Both *s*- and *p*-wave systems can support Majorana bound states for certain ranges of their external and material parameters, thus allowing for a switch in ground state fermion parity as an external parameter is varied.

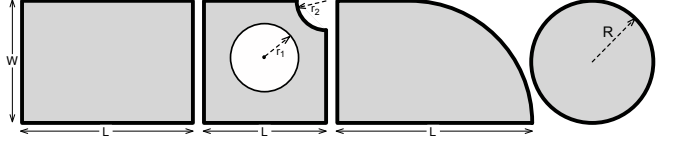


FIG. 1. The 2D geometries considered in the TB numerical simulations: a) Rectangle, b) Lorentz gas cavity, c) Quarter-stadium cavity, d) Disk.

III. PARITY CROSSINGS FOR MAJORANA BILLIARDS

A. Mapping to the Weyl problem

We start by considering the parity crossings of the *p*-wave Hamiltonian of Eq. (2), as the discussion is simpler. The parity crossing points μ_i are the chemical potential values for which two eigenstates of the *p*-wave Hamiltonian cross at zero energy, i.e. $H_p|_{\mu=\mu_i} \chi = 0$ for nontrivial χ . We define the density of crossings as $\rho(\mu) = \sum_i \delta(\mu - \mu_i)$, and investigate the asymptotic behavior of $\rho(\mu)$ as well as the related quantity $\mathcal{N}(\mu) = \int_{-\infty}^{\mu} \rho(\mu') d\mu'$, the number of crossing points below μ , for large μ . As is the case for the density of states, we distinguish the average density of crossings $\bar{\rho}$ and its oscillations ρ_{osc} and write $\rho(\mu) = \bar{\rho}(\mu) + \rho_{\text{osc}}(\mu)^{3-7}$. We consider these two terms separately below.

We start by mapping the problem of finding the parity crossing points to that of finding eigenvalues of a non-Hermitian operator by premultiplying Eq. (2) with τ_z :

$$\left(\frac{(\mathbf{p} + i m \Delta' \boldsymbol{\eta})^2}{2m} + V(\mathbf{r}) + m \Delta'^2 \right) \chi = \mu \chi, \quad (3)$$

where $\boldsymbol{\eta} = \tau_y \hat{x} - \tau_x \hat{y}$. We identify this operator as the Hamiltonian of a Rashba 2DEG with an imaginary Rashba parameter $\alpha = i \Delta'$. The real eigenvalues of this operator are the crossing points of the original Hamiltonian whereas the complex eigenvalues are associated with avoided crossings. While there is no general reason to assume that a given eigenvalue is real, in the limit of at least one of the system size parameters W (the “width”, along a direction which we choose to call the *y*-axis) is much smaller than the coherence length $\xi = \hbar/m\Delta'$, almost all eigenvalues of this operator are real. Rescaling the eigenfunction $\chi = e^{\boldsymbol{\eta} \cdot \mathbf{r} / \xi - \tau_z^2 / \xi^2} \tilde{\chi}$ and expanding in powers of W/ξ , we obtain⁷⁷

$$\left(\frac{(\mathbf{p} + \frac{2m^2 \Delta'^2}{\hbar} (\hat{\mathbf{z}} \times \mathbf{r}) \tau_z)^2}{2m} + V(\mathbf{r}) + m \Delta'^2 \right) \tilde{\chi} = \mu \tilde{\chi}. \quad (4)$$

We see that the crossing points are eigenvalues of the normal state Hamiltonian with fictitious magnetic field $\pm 2m^2 \Delta'^2 / e\hbar$ and constant potential shift $m \Delta'^2$. We note that the energy levels are even functions of applied magnetic fields. Therefore, to the order we are working in,

the effect of the fictitious magnetic field on the crossing points can be ignored as they only serve to modify the nonzero split in energy levels. We thus arrive at the remarkable result that the values of all parity crossing points are simply energy eigenvalues of the *normal state* Hamiltonian $H_N = p^2/2m + V(\mathbf{r}) + m\Delta'^2$. This identification allows us to map the average density of parity crossings to the conventional density of states of a normal state Hamiltonian. Well known results, such as the Weyl expansion^{1–3} (or for soft confinement the Thomas-Fermi approximation⁴) for the asymptotic DOS; Gutzwiller's trace formula in billiards for oscillations in DOS^{7,70,78–80}; the theory of Lifshitz tails^{81,82,92} for disordered systems; as well as the random matrix theory results for DOS fluctuations^{21,84}, carry over to the spectra of parity crossings.

For the average density of parity crossings for the p -wave system $\bar{\rho}_{w,p}(\mu)$ in d dimensions, we obtain:

$$\bar{\rho}_{w,p}(\mu) = \begin{cases} \frac{L}{2\pi\sqrt{\mu}} + \mathcal{O}(1) & \text{if } d = 1 \\ \frac{S}{4\pi} - \frac{\partial S}{8\pi\sqrt{\mu}} & \text{if } d = 2 \\ \frac{V\sqrt{\mu}}{4\pi^2} - \frac{\partial V}{16\pi} & \text{if } d = 3, \end{cases} \quad (5)$$

where L is the length of the 1D wire, S and ∂S are respectively the area and perimeter of the 2D billiard, and V and ∂V the volume and surface area of the 3D dot cavity respectively. In order to demonstrate our analytical results above for average density, we perform tight-binding simulations of parity crossings in a p -wave MB using the Kwant toolbox for quantum transport⁹⁰ (see Appendix A). Our results for a 2D MB are presented in Fig. 2a and b, where we plot $\mathcal{N}(\mu)$ both as derived from Eq. (5) (dashed lines) and as obtained from the TB simulation (solid, stepped lines). We see that the results fit well once the boundary corrections in Eq. (5) are taken into account. We note that there are no fitting parameters in the analytical plots. For a one dimensional disordered wire, we notice parity crossings in the fully depleted wire caused by rare disorder configurations (Fig. 2c). We identify these as analogous to the states that form the well known Lifshitz tail (see Appendix D)^{81,82,92}.

We next consider the case of the s -wave system described by the Hamiltonian H_s in Eq. (1) where we have two external parameters, namely μ and B . We follow Ref.^{77,86} to again transform the usual eigenvalue problem to a non-Hermitian one at zero energy and obtain:

$$(h(\mathbf{p}, \mathbf{r})\sigma_z - i\alpha p_x\sigma_x \mp B \mp \Delta\sigma_x)\phi_{\pm} = 0. \quad (6)$$

Here, we have ignored the chiral symmetry breaking term $i\alpha p_y\sigma_y$, which is a valid approximation in the limit $W \ll \xi$. For a finite system, the solution that satisfies all boundary conditions can be expressed in terms of the eigenfunctions of the normal state Hamiltonian $h\psi_n = (E_n - \mu)\psi_n$

$$\phi_{n,\pm} = \zeta_{\pm} e^{\pm x/\xi} \psi_n, \quad (7)$$

where $\zeta_{\pm}(\epsilon)$ are the eigenvectors of the 2×2 matrix $(E_n - \mu)\sigma_z \mp \Delta\sigma_x$ with eigenvalue $\pm\sqrt{(E_n - \mu)^2 + \Delta^2}$.

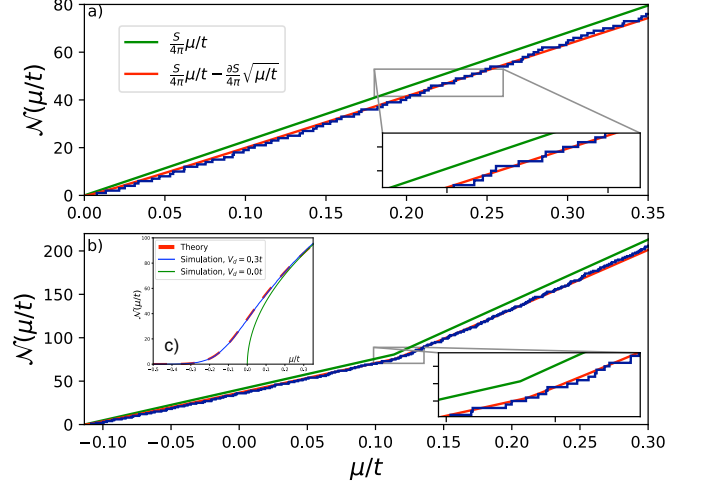


FIG. 2. (Color online) $\mathcal{N}(\mu/t)$ for a ballistic quarter stadium MB (see Fig. 1c). The green line is to the first term in the Weyl expansion whereas the red line includes the surface corrections. The staircase plot is the result of TB simulations. Lower-right insets are zoom-ins to show the fit between TB simulation and theory. a) p -wave MB with $L = 80a$, $W = 40a$ and $\Delta' = 0.001ta$. b) s -wave MB with $L = 100a$, $W = 50a$, $B = 0.23t$, $\Delta = 0.2t$ and $\alpha = 0.001ta$. The kink in the plot is at $\mu = \epsilon$ and signals the entrance of the second spin band into the picture. c) $\mathcal{N}(\mu/t)$ vs μ/t for a disorder averaged (200 realizations) 1D p -wave MB with $L = 500a$ and $\Delta' = 0.001ta$. The theory^{82,92} and the TB simulation results are shown (see Appendix D for further details).

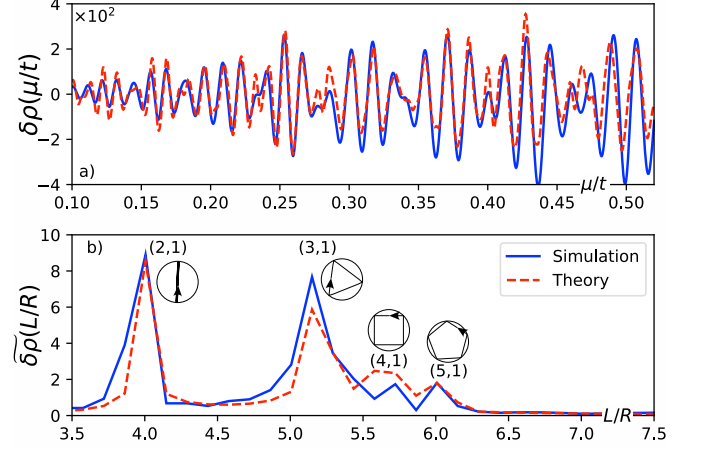


FIG. 3. (Color online) a) Density oscillations of parity crossings ρ_{osc} for a clean p -wave disk MB with $R = 100a$, $\Delta' = 0.001ta$. b) The Fourier transform of ρ_{osc} . The (v, w) pairs and corresponding classical orbits for the peaks are labeled. The smoothing parameter for both figures is $\gamma = 0.4/R$.

Substituting into Eq. (6), we find that the zero mode solutions (hence the parity crossings) happen on the curves in the $B - \mu$ plane⁸⁷ that satisfy

$$B^2 = (\mu - E_n)^2 + \Delta^2, \quad (8)$$

for a given eigenvalue E_n of the spinless single particle

Hamiltonian $h(\mathbf{p}, \mathbf{r})$. Hence, the density of parity crossing points (either in μ or B) can be obtained by analyzing the set of eigenvalues $\{E_n\}$ of $h(\mathbf{p}, \mathbf{r}) - \mu$. Noting that $h(\mathbf{p}, \mathbf{r})$ is the same for s - and p -wave cases, we write the s -wave Weyl expansion for $\rho_{w,s}(\mu)$ and $\rho_{w,s}(B)$ for parity crossing densities in terms of their p -wave counterpart $\rho_{w,p}(\mu)$ in Eq. (5):

$$\rho_{w,s}(\mu, B) = \sum_{s=\pm 1} \rho_{w,p}(\mu + \varsigma\epsilon(B)) \theta(\mu + \varsigma\epsilon(B)). \quad (9)$$

The asymptotic mean spacing $\langle \delta\mu \rangle = \rho_{w,s}^{-1}(\mu)$ or $\langle \delta B \rangle = \rho_{w,s}^{-1}(B)$ between crossing points can be obtained by inverting these expressions.

B. Oscillations in density of parity crossing points

We next investigate the oscillatory behavior of the density of parity crossings for a p -wave MB, due to interference between the actions of periodic semiclassical paths, as described by Gutzwiller's trace formula for billiards^{7,70,78–80}. We again take advantage of the parity crossing density being given by the normal state Hamiltonian, essentially adapt the discussion in Ref.⁴ to the case of the clean p -wave system and obtain its oscillatory part as:

$$\rho_{\text{osc}}(\mu) = \frac{2m}{(2\pi\hbar)^{3/2}p} \sum_{\text{po}} \mathcal{A}_{\text{po}} \cos \left[\frac{1}{\hbar} S_{\text{po}}(\mu) - \phi_{\text{po}} \right], \quad (10)$$

where the sum is over classical periodic orbits, the amplitude \mathcal{A}_{po} is given by $\mathcal{A}_{\text{po}} = \int_{\text{po}} |\mathcal{J}_{\text{po}}|^{-1/2} dr_{\parallel} dr_{\perp}$, S_{po} is the classical action over the orbit in question and $\phi_{\text{po}} = \sigma_{\text{po}}\pi/2 + \pi/4$ is the associated phase of the orbit with σ_{po} as the Maslov index. r_{\parallel} (r_{\perp}) are the coordinates parallel (perpendicular) to the orbit, and $\mathcal{J}_{\text{po}} = (\partial r_{\perp}/\partial p'_{\perp})_{\text{po}}$ quantifies the stability of the orbit with initial momentum \mathbf{p}' and final position \mathbf{r} considering only perturbations perpendicular to the trajectory.

We now exemplify this result by considering a clean disk p -wave MB and compare the theory to TB simulations.⁸⁸ In Fig. 3a, we plot the oscillatory part of the density of parity crossings ($\rho_{\text{osc}}(\mu)$) as a function of μ , as derived by Gutzwiller's trace formula and as given by our numerical simulations and show that the results fit well (without any fitting parameters). (Both the simulation results and the theory are smoothed using a Gaussian.) In Fig. 3b, we plot the Fourier transform of the above plot ($\tilde{\rho}_{\text{osc}}(L/R)$ where L is the length of the orbit and R is the radius of the disk). We identify the peaks in this plot corresponding to the lengths of the classical periodic orbits $L_{vw} = 2vR \sin(\varphi_{vw})$, where $\varphi_{vw} \equiv \pi w/v$ and the two integers v, w are the number of vertices and windings of the orbit, respectively.

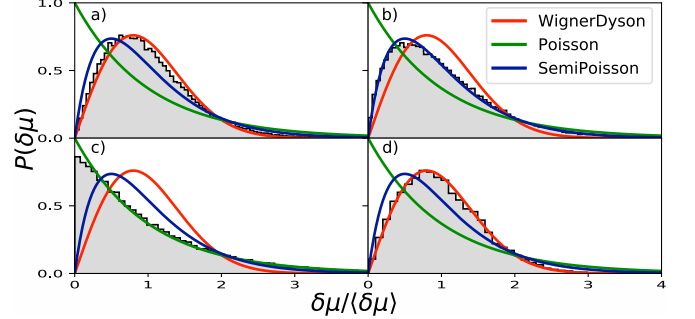


FIG. 4. (Color online) a-c) Level spacing distributions for a disordered rectangular p -wave MBs of varying lengths, averaged over 500 disorder realizations, with $\Delta' = 0.025ta$, disorder strength $V_d = 0.5t$, width $W = 20a$. a) $L = 40a < \xi$, b) $L = 100a \gtrsim \xi$ and c) $L = 1600a \gg \xi$, with $\xi = 80a$ being the coherence length. d) Level spacing distributions, averaged over 225 cavity realizations, for a clean p -wave Lorentz cavity MB. Here, $\Delta' = 0.001ta$, $L = 50a$, $W = 50a$, and $r_1 = r_2 = 10a$. The values of L/ξ in panels a)-d) are 0.5, 1.25, 20 and 0.4, respectively.

IV. UNIVERSAL FLUCTUATION STATISTICS OF PARITY CROSSING SPACINGS

We now focus on how the parity crossings are correlated. If at least one of the system size parameters (the “width”) becomes smaller than the coherence length, we find that the distribution of spacings, while universal, depends on whether the underlying normal system is regular, diffusive, chaotic or localized^{21,84}. For crossing spacings smaller than the normal state Thouless energy, the parity crossing points are described by an ensemble of real Hermitian random matrices, namely the orthogonal ensemble. The corresponding distribution of crossing spacings is given by the Wigner-Dyson distribution^{8,10–13}. Hence, the probability density $P(\delta\mu)$ associated with obtaining a crossing spacing of $\delta\mu$ is:

$$P(\delta\mu) = \frac{\pi\delta\mu}{2\langle\delta\mu\rangle} \exp \left(-\frac{\pi\delta\mu^2}{4\langle\delta\mu\rangle^2} \right) \quad (11)$$

When the mean crossing spacing is much bigger than the Thouless energy, the normal state is localized and the level spacing distribution is Poissonian:

$$P(\delta\mu) = \exp(-\delta\mu/\langle\delta\mu\rangle). \quad (12)$$

When the localization length is comparable to the system size, the normal state system is near the Anderson phase transition, the states are forced to overlap, leading to linear level repulsion for small spacings that turn into an exponential tail for larger energy spacings^{21,84}, signaling the fractal structure of the Majorana wavefunction:

$$P(\delta\mu) = \frac{\delta\mu}{\langle\delta\mu\rangle} \exp(-2\delta\mu/\langle\delta\mu\rangle). \quad (13)$$

We again simulate these cases with a TB model and plot the results against the probability distribution functions in Eq. (11), (12) and (13). Fig. 4 (Fig. 5) shows our

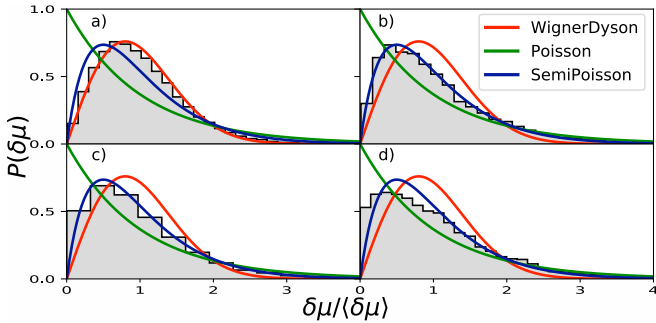


FIG. 5. (Color online) a-c) Level spacing distributions for disordered rectangular *s*-wave MBs with increasing Zeeman energy B , averaged over 500 disorder realizations, with $L = 200a$, $W = 10a$, $V_d = 0.2t$, $\alpha = 0.025ta$, $\Delta = 0.12t$, and a) $B = 1.12t$, b) $B = 0.22t$ and c) $B = 0.13t$. d) Level spacing distributions for clean *s*-wave Lorentz cavity MB, averaged over 225 cavity realizations. Here, $\alpha = 0.001ta$, $\Delta = 0.2t$, $B = 0.23t$, $L = 50a$, $W = 50a$, and $r_1 = r_2 = 10a$. The values of L/ξ in panels a)-d) are 0.27, 1.63, 6.1 and 0.04, respectively.

p-wave (*s*-wave) results for disordered rectangle cavities (a-c) and chaotic billiards (d). In line with the above prediction, the distributions evolve from Wigner-Dyson to semi-Poissonian to Poissonian as the system goes from localized to diffusive, and fit the respective distributions well without any fitting parameters (see Fig. 4 and Appendix A). We note, however, that in the *s*-wave case, $P(\delta\mu \rightarrow 0)$ approaches 0.5 if both spin species are populated. This is understood by considering the parity crossing points as two interlaced sequences belonging to different spin species⁸⁶ for larger B . The elements of each sequence feature level repulsion, and one sequence is the same as the other sequence, but shifted (by the Zeeman energy). For large enough shifts two sequences become uncorrelated, suppressing the level repulsion between half the levels. This leads to the value 0.5 for the spacing distribution function at zero. (See Appendix E for further discussion on the universality crossover for Figures 4a)-d) and 5a)-d).)

V. CONCLUSIONS

We show that the set of external parameters at which the ground state fermion parity of a Majorana billiard switches (the “spectrum” of the MB) is subject to well-known asymptotic analysis of eigenvalues of the Laplacian operator having disorder or chaotic dynamics. In particular, we show that the mean density of crossings obey a Weyl expansion, and has a Lifshitz tail in the disordered case. Moreover, we demonstrate that the oscillations of the density of parity crossings can be obtained by semiclassical means extending Gutzwiller’s trace formula to Majorana billiards. Finally, we show that the spacing fluctuations of parity switches obey a universal

distribution, as described by random matrix theory. We thus demonstrate that “one can hear (information about) the shape of a Majorana billiard.”

ACKNOWLEDGMENTS

We thank M. Wimmer, K. Richter and C.W.J. Beenakker for useful discussions. This work was supported by funds of the Erdal İnönü chair. İ.A. is a member of the Science Academy–Bilim Akademisi–Turkey; B.P. and A.M.B thank the Science Academy–Bilim Akademisi–Turkey for the use of their facilities throughout this work.

Appendix A: Numerical calculation of the parity crossing points using tight-binding approximation

For the *p*-wave numerical results, we start with the LHS of Eq. (3), which is a non-Hermitian operator, as opposed to the *p*-wave Hamiltonian in Eq. (2). This non-Hermitian operator and the *p*-wave Hamiltonian are equivalent in the sense that no approximation was made in going from Eq. (2) to Eq. (3). We form the tight-binding (TB) form of this operator using conventional methods (see, for example,⁸⁹):

$$\begin{aligned} \hat{O}_{\text{TB}}^{\text{PW}} = & (2dt + V(x, y)) \tau_0 |x, y\rangle \langle x, y| \\ & - t\tau_0 [|x+a, y\rangle \langle x, y| + |x, y+a\rangle \langle x, y| + \text{h.c.}] \\ & + i\Delta' \left[\frac{i}{2}\tau_y |x+a, y\rangle \langle x, y| \right. \\ & \left. - \frac{i}{2}\tau_x |x, y+a\rangle \langle x, y| + \text{h.c.} \right], \end{aligned} \quad (\text{A1})$$

where $t = \hbar^2/2ma^2$ is the hopping parameter, a is the lattice constant for the TB lattice and $V(x, y)$ is the onsite potential. For disordered systems, we take the disorder to be Gaussian, i.e. $\langle V(\mathbf{r})V(\mathbf{r}')\rangle = D\delta(\mathbf{r} - \mathbf{r}')$ for \mathbf{r}, \mathbf{r}' within the system, where $\langle \dots \rangle$ represents averaging over disorder realizations, $D \equiv V_d^2 a^d$ with V_d is the disorder strength and d is the dimension of the system ($d = 2$ in most of our manuscript; if $d = 1$, then the hoppings in the *y*-direction are absent). In TB simulations, this corresponds to choosing randomly the on-site potential from a Gaussian distribution. For ballistic cavity results, we set $V(x, y) = 0$ within the cavity. The boundaries of the system are defined by the lack of hopping to outside. We form the TB sparse matrix of this operator using the Kwant library⁹⁰ over the system shape which described in Fig. 1 and the relevant plots. We then numerically obtain the eigenvalues of this (non-Hermitian) sparse matrix using LAPACK libraries present in the SciPy package⁹¹. We finally discard non-real eigenvalues to obtain our results.

For the *s*-wave results, we go through the same procedure, except for utilizing the appropriate TB-representation of the non-Hermitian operator derived

from the Hamiltonian in Eq. (1). For $E = 0$, the TB model for the s -wave equivalent of Eq. (3) reads $\hat{O}_{\text{TB}}^{\text{SW}}\chi = \mu\chi$, with the non-Hermitian operator $\hat{O}_{\text{TB}}^{\text{SW}}$ defined as:

$$\begin{aligned} \hat{O}_{\text{TB}}^{\text{SW}} = & \left[(2dt + V(x, y)) \sigma_0 \tau_0 + B \sigma_x \tau_z \right] |x, y\rangle \langle x, y| \\ & - t \sigma_0 \tau_0 [|x+a, y\rangle \langle x, y| + |x, y+a\rangle \langle x, y| + \text{h.c.}] \\ & - \sigma_y \tau_0 \left[\frac{i\alpha}{2} |x+a, y\rangle \langle x, y| + \text{h.c.} \right] \\ & + \sigma_x \tau_0 \left[\frac{i\alpha}{2} |x, y+a\rangle \langle x, y| + \text{h.c.} \right] \\ & + i\Delta \sigma_0 \tau_y |x, y\rangle \langle x, y|. \end{aligned} \quad (\text{A2})$$

Again, in the plots where $d = 1$, the hoppings in the y -direction are absent.

For disorder averaging, we create many realizations of the same disordered system and do statistics over the combined results of each realization. For shape averaging over chaotic cavities, we create many realizations of the same chaotic cavity, the difference between realizations being the positioning of a relevant geometrical feature of the cavity, without changing the size of the system volume or boundary. For the Lorentz cavity, for example, we slightly change the position of the central stopper for each realization (making sure the stopper never comes too close to a wall). We make sure the change is large enough numerically to yield a completely different set of eigenvalues.

Appendix B: Universal spectra of parity crossing points in s -wave systems

In this section, we note that for a given disorder realization in a given s -wave system, the placement of the parity crossing points as a function of $\mu + \sqrt{B^2 - \Delta^2}$ is universal as other system parameters are varied, as indicated in Eq. (8). In Fig. 6, we plot the first four eigenvalues of an s -wave system with a specific disorder realization for different values of μ and Δ as a function of B in Fig. 6(a) and as a function of $\mu + \sqrt{B^2 - \Delta^2}$ in Fig. 6(b). We see that in the latter case, all crossings happen at the same points for all parameters. Another salient point seen in Fig. 6 is that the particle-hole symmetry assures another state will cross zero at the same point; level repulsion does not occur because of this symmetry.

Appendix C: Oscillatory behavior of the density of parity crossings in a disk Majorana billiard

In this section, we derive the oscillatory part of the density of parity crossings for a p -wave system on a two dimensional disk MB lattice of radius R , due to the action of the high-symmetry periodic orbits according to Gutzwiller's trace formula⁴. We adapt the continuum version of the 2D disk billiard solutions to our TB simulations in order to show a better fit between theory

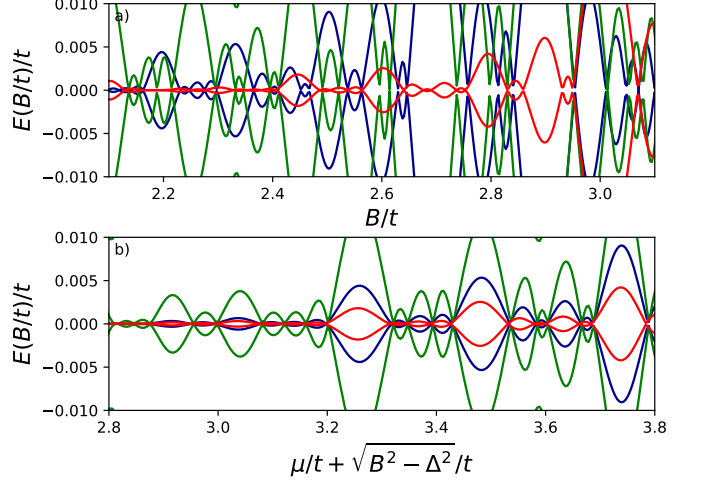


FIG. 6. (Color online) A plot of the lowest four eigenvalues of the disordered s -wave Hamiltonian in Eq. (1), discretized on a 1D lattice of 100 sites, plotted as a function of (a) B/t and (b) $\mu/t + \sqrt{B^2 - \Delta^2}/t$, for different values of Hamiltonian parameters. In both plots, the green set of curves represents the lowest four eigenvalues obtained for $\Delta = 1.5t$, $\alpha = 0.05ta$, $\mu = 1.8t$; the blue set is for $\Delta = 1.8t$, $\alpha = 0.05ta$, $\mu = 2.0t$; and the red set is for $\Delta = 1.8t$, $\alpha = 0.08ta$, $\mu = 1.6t$. Here, $t = \hbar^2/2ma^2$ is the hopping parameter. In all cases, the same disorder realization with a disorder strength $V_d = 0.5t$ is taken.

and simulation. In the TB case, we obtain the classical action of a given orbit from the lattice Hamiltonian $H_{\text{lat}} = 2t(1 - \cos(pa/\hbar))$ as

$$S_{vw} = \left(p - \frac{\hbar}{a} \tan\left(\frac{pa}{2\hbar}\right) \right) L_{vw}, \quad (\text{C1})$$

where $L_{vw} = 2vR \sin(\varphi_{vw})$ is the classical orbit length, $\varphi \equiv \pi w/v$ is half of the polar angle and p is the momentum of the particle. v, w are two integers which correspond to the number of vertices and windings of the classical orbit in question, respectively. The oscillatory part $\rho_{\text{osc}}(E)$ of the density of states $\rho(E)$ at a given energy is given as⁴:

$$\begin{aligned} \rho_{\text{osc}}(E) = & \frac{1}{E_0} \sqrt{\frac{\hbar}{\pi p R}} \sum_{w=1}^{\infty} \sum_{v=2w}^{\infty} f_{vw} \frac{\sin^{3/2}(\varphi_{vw})}{\sqrt{v}} \\ & \times \text{Im}[\exp\{i(S_{vw}/\hbar - 3v\pi/2 + 3\pi/4)\}], \end{aligned} \quad (\text{C2})$$

with

$$f_{vw} = \begin{cases} 1 & \text{if } v = 2w \\ 2 & \text{if } v > 2w \end{cases} \quad (\text{C3})$$

and $E_0 \equiv \hbar^2/(2mR^2)$.

For the TB case, we start from $h(p, \mathbf{r})$ of Eq. (2) with $V(\mathbf{r}) = 0$. Then, the TB version of the momentum is given by

$$p(E, \mu) = \frac{\hbar}{a} \arccos\left(1 - \frac{E + \mu}{2t}\right), \quad (\text{C4})$$

where E labels the energy levels of the system. We now use the fact that the parity crossing points μ_c are the eigenvalues of the normal state Hamiltonian and obtain the oscillatory part of the density of parity crossings:

$$\begin{aligned} \rho_{\text{osc}}(\mu) &= \frac{1}{E_0} \left(\frac{\hbar}{\pi R p(0, \mu)} \right)^{1/2} \sum_{w=1}^{\infty} \sum_{v=2w}^{\infty} f_{vw} \frac{\sin^{3/2}(\varphi_{vw})}{\sqrt{v}} \\ &\times \text{Im} \left[\exp \left\{ i L_{vw} \left(\frac{p(i\gamma, \mu)}{\hbar} - \frac{1}{a} \tan \frac{p(i\gamma, \mu) a}{2\hbar} \right) \right. \right. \\ &\left. \left. + i(-3v\pi/2 + 3\pi/4) \right\} \right]. \end{aligned} \quad (\text{C5})$$

Here, we combined Eq. (C1), (C2) and (C4) at $E = 0 + i\gamma$, with γ being the smoothing parameter.

To obtain the numerical ρ_{osc} and $\tilde{\rho}_{\text{osc}}$ plots in Fig. 3, we set up the TB p -wave system on a circle and obtain the parity crossing points μ_c using the Kwant toolbox as described in the above SOM section. We then obtain the oscillatory part of the smoothed density ρ_{osc} as

$$\begin{aligned} \rho_{\gamma}(\mu/t) &= \int d\mu' \sum_{\mu_c} \delta(\mu' - \mu_c) F\left(\frac{\mu - \mu'}{\gamma}\right) \\ \rho_{\text{osc}}(\mu/t) &= \rho_{\gamma}(\mu/t) - \rho_w(\mu/t) \end{aligned} \quad (\text{C6})$$

where $F\left(\frac{\mu - \mu'}{\gamma}\right)$ is the smoothing function, which we choose to be Gaussian, γ is the smoothing parameter (the width of the Gaussian), ρ_{γ} is the smooth part of the density of parity crossings and ρ_w corresponds to the volume and surface terms of the Weyl expansion in Eq. (5). We then take the Fourier transform of $\rho_{\text{osc}}(k(\mu/t) a) \xrightarrow{\text{FT}} \tilde{\rho}_{\text{osc}}(L/R)$ to identify the peaks corresponding to the lowest length L and the highest symmetry semiclassical periodic orbits⁴ and plot the results in Fig. 3b.

Appendix D: Lifshitz tail in disordered Majorana billiards

Disordered systems feature states below zero energy due to the presence of islands with an average of below zero potential, even though the average potential for the whole system is zero. Called the Lifshitz tail, this phenomenon is present also in MBs (see Fig. 7). The overall disorder-averaged integrated density of parity crossings for a 1D p -wave MB with Gaussian disorder $\langle V(\mathbf{r})V(\mathbf{r}') \rangle = D\delta(\mathbf{r} - \mathbf{r}')$ is given by the formula⁹²:

$$\mathcal{N}(\mu) = \frac{\kappa_0}{\pi^2 \varepsilon_0} \frac{1}{[\text{Ai}(-2\mu/\varepsilon_0)]^2 + [\text{Bi}(-2\mu/\varepsilon_0)]^2}, \quad (\text{D1})$$

where Ai and Bi are the Airy functions, $\varepsilon_0 = (D^2 m \hbar^{-2})^{1/3}$ and $\kappa_0 = (D m^2 \hbar^{-4})^{1/3}$.

In Fig. 7, we plot Eq. (D1) and TB simulations for a disordered system (and a clean TB system for comparison). We note that the theory and the numerical simulations fit very well without any fitting parameters.

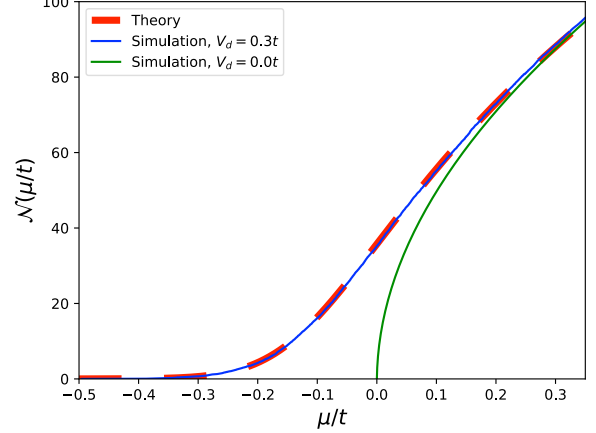


FIG. 7. (Color online) $\mathcal{N}(\mu/t)$ vs. μ/t for a 1D p -wave 1D MB for a wire of length $500a$ and $\Delta' = 0.001ta$. For the disordered case, the TB simulation plot is the average of 200 realizations. The theory lines are the plots of Eq. (D1) for $V_d = 0.0t$ and $V_d = 0.3t$. No fitting parameters are used.

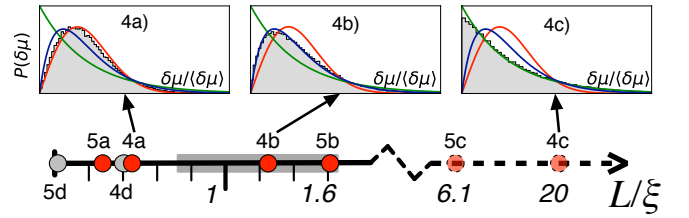


FIG. 8. (Color online) The L/ξ values for Figures 4a)-d) and 5a)-d). The shaded area around $L/\xi = 1$ schematically represents the universality crossover region where the statistics are sub-Poissonian. Three panes from Figure 4 are reproduced as an example of Gaussian, sub-Poissonian and Poissonian statistics. Points corresponding to Figures 4d) and 5d) are shaded differently as a reminder that due to the cavity geometry, the exact value of L is not immediately obvious; the length of one side of the Lorentz cavity was used for this value (see Figure 1).

Appendix E: Universality class crossovers of disordered p -wave Majorana billiards

In this Appendix section, we summarize the values of L/ξ for the systems depicted in Figures 4a)-d) and 5a)-d), as well as one additional 2D p -wave system where both dimensions are larger than ξ . In Figure 8, we note the locations of all of the Figures 4a)-d) and 5a)-d) on the L/ξ axis. These systems all have one dimension (say, W) much smaller than ξ , thus exemplifying systems that satisfy the approximation requirement for the mapping described in Section III A. We again note that the numerical simulations depicted here do not use this approximation and simulate the full TB version of the Bogoliubov-de Gennes Hamiltonian (see Appendix A). Figure 8 clearly shows the universality crossover in these systems. In Fig-

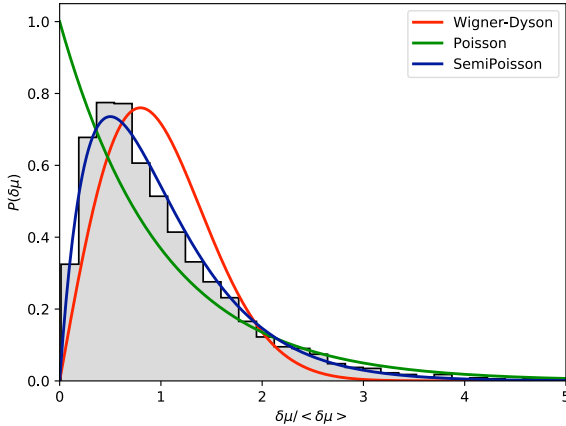


FIG. 9. (Color online) Parity crossing distance statistics for a p -wave system with *both* dimensions much larger than ξ ($L = W = 5\xi$, showing the statistics obtained from a TB simulation of a disordered system in a square geometry (500 disorder realizations) whose parameters are $L = W = 80a$, $V_0 = 0.32t$, $\Delta' = 0.125ta$ and $\xi = 16a$.

¹ H. Weyl and K. Chandrasekharan *Gesammelte Abhandlungen I*, v.4 (Springer Berlin Heidelberg, 1968).

² H. Baltes and E. Hilf, *Spectra of finite systems: a review of Weyl's problem, the eigenvalue distribution of the wave equation for finite domains and its applications on the physics of small systems* (Bibliographisches Institut, 1976).

³ R. Balian and C. Bloch, *Annals of Physics* **60**, 401 (1970).

⁴ M. Brack and R. K. Bhaduri, *Semiclassical Physics*, (Westview, Boulder, Colo., 2003).

⁵ R. Balian and C. Bloch, *Annals of Physics* **69**, 76160 (1972).

⁶ M. V. Berry, *Proc. R. Soc. of London. Series A, Mathematical and Physical Sciences* **400**, 229 (1985).

⁷ M. C. Gutzwiller, *Chaos in Classical and Quantum Mechanics*, (Springer, New York, 1990).

⁸ M. Mehta, *Random Matrices*, Pure and Applied Mathematics (Elsevier Science, 2004).

⁹ J. Wurm, A. Rycerz, İ. Adagideli, M. Wimmer, K. Richter, and H. U. Baranger, *Phys. Rev. Lett.* **102**, 056806 (2009).

¹⁰ E. P. Wigner, *Annals of Mathematics* **62**, 548 (1955).

¹¹ F. J. Dyson, *Journal of Mathematical Physics* **3**, 1199 (1962).

¹² F. J. Dyson, *Journal of Mathematical Physics* **3**, 157165 (1962).

¹³ F. J. Dyson and M. L. Mehta, *Journal of Mathematical Physics* **4**, 701712 (1963).

¹⁴ O. Bohigas, M. J. Giannoni, and C. Schmit, *Phys. Rev. Lett.* **52**, 1 (1984).

¹⁵ A. V. Balatsky, I. Vekhter, and J.-X. Zhu, *Rev. Mod. Phys.* **78**, 373 (2006).

¹⁶ S. Mi, D.I. Pikulin, M. Marciani, and C.W.J. Beenakker, *J. Exp. Theor. Phys.* **119**, 1018 (2014).

¹⁷ L. Fu and C. L. Kane, *Physical Review B* **79**, 161408(R) (2009).

¹⁸ S. Ryu, A. P. Schnyder, A. Furusaki, and A. W. W. Ludwig, *New Journal of Physics* **12**, 065010 (2010).

¹⁹ T. D. Stanescu, R. M. Lutchyn, and S. Das Sarma, *Phys. Rev. B* **84**, 144522 (2011).

²⁰ E. J. H. Lee, X. Jiang, R. Aguado, G. Katsaros, C. M. Lieber, and S. De Franceschi, *Phys. Rev. Lett.* **109**, 186802 (2012).

²¹ C. W. J. Beenakker, J. M. Edge, J. P. Dahlhaus, D. I. Pikulin, S. Mi, and M. Wimmer, *Phys. Rev. Lett.* **111**, 037001 (2013).

²² M.-T. Rieder, P. W. Brouwer, and İ. Adagideli, *Phys. Rev. B* **88**, 060509(R) (2013).

²³ W. Chang, V. E. Manucharyan, T. S. Jespersen, J. Nygård, and C. M. Marcus, *Phys. Rev. Lett.* **110**, 217005 (2013).

²⁴ J. D. Sau and E. Demler, *Phys. Rev. B* **88**, 205402 (2013).

²⁵ D. M. Badiane, L. I. Glazman, M. Houzet, and J. S. Meyer, *Comptes Rendus Physique* **14**, 840856 (2013).

²⁶ D. Chevallier, P. Simon, and C. Bena, *Phys. Rev. B* **88**, 165401 (2013).

²⁷ E. J. H. Lee, X. Jiang, M. Houzet, R. Aguado, C. M. Lieber, and S. De Franceschi, *Nat. Nano.* **9**, 79 (2014).

²⁸ S. Hegde, V. Shivamoggi, S. Vishveshwara, and D. Sen, *New J. Phys.* **17**, 053036 (2015).

²⁹ A. Y. Kitaev, *Physics-Uspekhi* **44**, 131 (2001).

³⁰ M. Z. Hasan and C. L. Kane, *Rev. Mod. Phys.* **82**, 3045 (2010).

³¹ X.-L. Qi and S.-C. Zhang, *Rev. Mod. Phys.* **83**, 1057 (2011).

³² J. Alicea, *Reports on Progress in Physics* **75**, 076501 (2012).

³³ B. A. Bernevig and T. Hughes *Topological Insulators and Topological Superconductors* (Princeton University Press,

ure 9, we show the statistics of a system with both dimensions L_1 and L_2 much larger than ξ , corresponding to a real Hamiltonian with sub-Poissonian statistics²¹.

⁴¹ William Street, Princeton, New Jersey 08540, 2013).

³⁴ S. R. Elliott and M. Franz, Rev. Mod. Phys. **87**, 137 (2015).

³⁵ S. Das Sarma, J. D. Sau, and T. D. Stanescu, Phys. Rev. B **86**, 220506(R) (2012).

³⁶ R. Rodríguez-Mota, S. Vishveshwara, and T. Perego-Barnea, J. Phys. Chem. Solids **128**, 179-187 (2019).

³⁷ V. Mourik, K. Zuo, S. M. Frolov, S. R. Plissard, E. P. A. M. Bakkers and L. P. Kouwenhoven, Science **336**, 1003 (2012).

³⁸ S. Nadj-Perge, I. K. Drozdov, J. Li, H. Chen, S. Jeon, J. Seo, A. H. MacDonald, B. A. Bernevig and A. Yazdani, Science **346**, 602 (2014).

³⁹ A. Fornieri, A. M. Whiticar, F. Setiawan, E. P. Marín, A. C. C. Drachmann, A. Keselman, S. Gronin, C. Thomas, T. Wang, R. Kallaher, G. C. Gardner, E. Berg, M. J. Manfra, A. Stern, C. M. Marcus, and F. Nichele, Nature **569**, 8992 (2019).

⁴⁰ S. Vaitiekėnas, M.-T. Deng, P. Krogstrup, and C. M. Marcus, arXiv:1809.05513 (2018).

⁴¹ T.H. Hsieh and L. Fu, Phys. Rev. Lett. **108**, 107005 (2012).

⁴² E. Prada, P. San-Jose, and R. Aguado, Phys. Rev. B **86**, 180503(R) (2012).

⁴³ J.F. Silva and E. Vernek, Journal of Physics: Condensed Matter **28**, 435702 (2016).

⁴⁴ C.-X. Liu, J.D. Sau, T.D. Stanescu, and S. Das Sarma, Phys. Rev. B **96**, 075161 (2017).

⁴⁵ F. Nichele, A.C.C. Drachmann, A.M. Whiticar, E.C.T. O'Farrell, H.J. Suominen, A. Fornieri, T. Wang, G.C. Gardner, C. Thomas, A.T. Hatke, P. Krogstrup, M.J. Manfra, K. Flensberg, and C.M. Marcus, Phys. Rev. Lett. **119**, 136803 (2017).

⁴⁶ K. Zuo, V. Mourik, D.B. Szombati, B. Nijholt, D.J. van Woerkom, A. Geresdi, J. Chen, V.P. Ostroukh, A.R. Akhmerov, S.R. Plissard, D. Car, E.P.A.M. Bakkers, D.I. Pikulin, L.P. Kouwenhoven, and S.M. Frolov, Phys. Rev. Lett. **119**, 187704 (2017).

⁴⁷ H.-Z. Tang, Y.-T. Zhang, and J.-J. Liu, Physics Letters A **382**, 991 (2018).

⁴⁸ C. Moore, T.D. Stanescu, and S. Tewari, Phys. Rev. B **97**, 165302 (2018).

⁴⁹ M. Hell, K. Flensberg, and M. Leijnse, Phys. Rev. B **97**, 161401(R) (2018).

⁵⁰ C.-X. Liu, J. D. Sau, and S. Das Sarma, Phys. Rev. B **97**, 214502 (2018).

⁵¹ A. Vuik, B. Nijholt, A.R. Akhmerov, and M. Wimmer, arXiv:1806.02801 [cond-mat] (2018).

⁵² C. Moore, C. Zeng, T.D. Stanescu, and S. Tewari, Phys. Rev. B **98**, 155314 (2018).

⁵³ C. Reeg, O. Dmytruk, D. Chevallier, D. Loss, and J. Klinovaja, Phys. Rev. B **98**, 245407 (2018).

⁵⁴ M. Kayyalha, M. Kargarian, A. Kazakov, I. Miotkowski, V.M. Galitski, V.M. Yakovenko, L.P. Rokhinson, and Y.P. Chen, Phys. Rev. Lett. **122**, 047003 (2019).

⁵⁵ J. Chen, B. Woods, P. Yu, M. Hocevar, D. Car, S. Plissard, E. Bakkers, T. Stanescu, and S. Frolov, arXiv:1902.02773 [cond-mat] (2019).

⁵⁶ B. D. Woods, J. Chen, S.M. Frolov, and T.D. Stanescu, arXiv:1902.02772 [cond-mat] (2019).

⁵⁷ Z. Cao, H. Zhang, H.-F. Lü, W.-X. He, H.-Z. Lu, and X.C. Xie, Phys. Rev. Lett. **122**, 147701 (2019).

⁵⁸ O. Motrunich, K. Damle, and D.A. Huse, Phys. Rev. B **63**, 224204 (2001).

⁵⁹ P.W. Brouwer, M. Duckheim, A. Romito, and F. von Oppen, Phys. Rev. B **84**, 144526 (2011).

⁶⁰ P.W. Brouwer, M. Duckheim, A. Romito, and F. von Oppen, Phys. Rev. Lett. **107**, 196804 (2011).

⁶¹ D. I. Pikulin, J. P. Dahlhaus, M. Wimmer, H. Schomerus, and C. W. J. Beenakker, New Journal of Physics **14**, 125011 (2012).

⁶² M. Popinciuc, V.E. Calado, X.L. Liu, A.R. Akhmerov, T.M. Klapwijk, and L.M.K. Vandersypen, Phys. Rev. B **85**, 205404 (2012).

⁶³ D. Bagrets and A. Altland, Phys. Rev. Lett. **109**, 227005 (2012).

⁶⁴ J. Liu, A. C. Potter, K. T. Law, and P. A. Lee, Phys. Rev. Lett. **109**, 267002 (2012).

⁶⁵ P. Neven, D. Bagrets, and A. Altland, New J. Phys. **15**, 055019 (2013).

⁶⁶ H. O. H. Churchill, V. Fatemi, K. Grove-Rasmussen, M. T. Deng, P. Caroff, H. Q. Xu, and C. M. Marcus, Phys. Rev. B **87**, 241401(R) (2013).

⁶⁷ J.D. Sau and S. Das Sarma, Phys. Rev. B **88**, 064506 (2013).

⁶⁸ H. Pan, W.S. Cole, J.D. Sau, and S. Das Sarma, arXiv:1906.08193 [cond-mat] (2019).

⁶⁹ I. Kosztin, D. L. Maslov, and P. M. Goldbart, Phys. Rev. Lett. **75**, 1735 (1995).

⁷⁰ I. Adagideli and P. M. Goldbart, Int. J. Mod. Phys. B **16**, 1381 (2002).

⁷¹ C. W. J. Beenakker, in *Quantum Dots: A Doorway to Nanoscale Physics*, edited by W. Dieter Heiss (Springer Berlin Heidelberg, Berlin, Heidelberg, 2005), pp. 131174.

⁷² M. Kac, The American Mathematical Monthly **73**, 1 (1966).

⁷³ Although isospectral domains of different shapes exist⁹³, it turns out to be possible to extract geometrical and dynamical information from the energy spectra¹.

⁷⁴ P. G. deGennes, *Superconductivity of Metals and Alloys* (Westview Press, 1999).

⁷⁵ R. M. Lutchyn, J. D. Sau, and S. Das Sarma, Phys. Rev. Lett. **105**, 077001 (2010).

⁷⁶ Y. Oreg, G. Refael, and F. von Oppen, Phys. Rev. Lett. **105**, 177002 (2010).

⁷⁷ I. Adagideli, M. Wimmer, and A. Teker, Phys. Rev. B **89**, 144506 (2014).

⁷⁸ R. A. Jalabert, H. U. Baranger, and A. D. Stone, Phys. Rev. Lett. **65**, 2442 (1990).

⁷⁹ H. Ishio and J. Burgdörfer, Phys. Rev. B **51**, 2013 (1995).

⁸⁰ I. Adagideli and P. M. Goldbart, Phys. Rev. B **65**, 201306(R) (2002).

⁸¹ I. M. Lifshitz, Advances in Physics **13**, 483 (1964).

⁸² B. I. Halperin, Phys. Rev. **139**, A104 (1965).

⁸³ C. Itzykson and J.-M. Drouffe, *Statistical Field Theory v.2* (Cambridge University Press, Cambridge [England]; New York, 1989).

⁸⁴ C. W. J. Beenakker, Rev. Mod. Phys. **69**, 731 (1997).

⁸⁵ C. W. Groth, M. Wimmer, A. R. Akhmerov, and X. Waintal, New Journal of Physics **16**, 063065 (2014).

⁸⁶ B. Pekerten, A. Teker, O. Bozat, M. Wimmer, and I. Adagideli, Phys. Rev. B **95**, 064507 (2017).

⁸⁷ See App. B for the universality of the fermion parity crossing points for a given sample with different B and μ and for further details.

⁸⁸ See App. C for the adaptation of Eq. (10) to a 2D TB disk MB and for further details.

⁸⁹ S. Datta, *Electronic Transport in Mesoscopic Systems* (Cambridge University Press, 1997).

⁹⁰ C. W. Groth, M. Wimmer, A. R. Akhmerov, and X. Waintal, *New Journal of Physics* **16**, 063065 (2014).

⁹¹ E. Jones, E. Oliphant, P. Peterson et al. **SciPy: Open Source Scientific Tools for Python** (2001-) <http://www.scipy.org/> [Online; accessed 2018-04-01].

⁹² C. Itzykson and J.-M. Drouffe, *Statistical Field Theory* v.2 (Cambridge University Press, Cambridge [England]; New York, 1989).

⁹³ C. Gordon, D. Webb, and S. Wolpert, *Invent. Math* **110**, 1 (1992).